Düzce University Journal of Science & Technology

Research Article

Synthesis and Structural Characterization of Y-doped Pyramidal ZnO Powders

Hanifi KEBİROĞLU [a,*], Omer KAYGILI [a], Niyazi BULUT [a], Havva Esma OKUR [b], Ismail ERCAN [c], Filiz ERCAN [d], I.S. YAHIA [e,f], Tankut ATES [a], Suleyman KOYTEPE [g], Turgay SECKIN [g], Turan İNCE [a]

[a] *Department of Physics, Faculty of Science, Firat University, 23119 Elazig, TURKEY*
[b] *Department of Chemistry, Bursa Technical University, Bursa 16310, TURKEY*
[c] *Institute for Research and Medical Consultations (IRMC), Imam Abdulrahman Bin Faisal University, Dammam, SAUDI ARABIA*
[d] *College of Science, Imam Abdulrahman Bin Faisal University, P.O. Box 1982, Dammam, 31441, SAUDI ARABIA*
[e] *Advanced Functional Materials & Optoelectronic Laboratory (AFMOL), Department of Physics, Faculty of Science, King Khalid University, P.O. Box 9004, Abha, SAUDI ARABIA*
[f] *Nanoscience Laboratory for Environmental and Bio-medical Applications (NLEBA), Semiconductor Lab., Department of Physics, Faculty of Education, Ain Shams University, Roxy, 11757 Cairo, EGYPT*
[g] *Department of Chemistry, Faculty Science & Arts, Inonu University, 44280 Malatya, TURKEY*
DOI: 10.29130/dubited.655244

ABSTRACT

The present study focuses on the structural changes in ZnO powder induced by doping of a rare earth metal of Y. For this aim, we synthesized four ZnO samples with different Y-content using the combustion reaction method. X-ray powder diffraction (XRPD) technique and scanning electron microscopy (SEM) results confirm that the as-investigated structural parameters and morphology of the ZnO structure were affected directly by the concentration of Y dopant. For each Y-doped sample, randomly-oriented pyramidal morphology and the formation of a minority phase of Y_2O_3 were observed. A gradual increase in both lattice parameters and unit cell volume was detected with increasing Y content. All samples were found to be thermally stable in the temperature interval of 25-950 °C.

Keywords: *Morphology, Crystal structure, Zinc oxide (ZnO)*

Y Katkılı Piramit ZnO Tozlarının Sentez ve Karakterizasyonu

ÖZET

Mevcut çalışma, nadir toprak metali Y'un ZnO tozuna katkılanmasının meydana getirdiği yapısal değişikliklere odaklanmaktadır. Bu amaçla, farklı Y içeriğine sahip dört ZnO numunesi, yakma reaksiyon metodu kullanarak sentezledik. X-ışını toz kırınımı (XRPD) ve taramalı elektron mikroskopisi (SEM) sonuçları, ZnO'un araştırılan yapısal özellikleri ve morfolojisinin doğrudan Y katkısından etkilendiğini doğrulamaktadır. Her Y katkılı numune için, rasgele-yönelimli piramit şeklinde morfoloji ve Y_2O_3 azınlık fazının oluşumu gözlendi. Y içeriğinin artmasıyla hem örgü parametrelerinde hem de birim hücre hacminde kademeli bir düşüş tespit edildi. Tüm numunelerin 25–950 °C sıcaklık aralığında termal olarak kararlı olduğu bulundu.

Anahtar Kelimeler: *Morfoloji, Kristal yapı, Çinko oksit (ZnO)*

Received: 13/12/2019, Revised: 12/02/2020, Accepted: 08/04/2020

I. INTRODUCTION

There are several metal oxides (e.g., CuO, NiO, ZnO, and MgO) manufactured for different applications. They have many implementation areas in physics, chemistry and material science. Among these metal oxides, ZnO is one of the most promising materials for various technological applications.

ZnO is a well-known n-type II-VI semiconducting compound having piezoelectric, dielectric properties with a wide band gap of 3.37 eV and a large exciton binding energy of 0.06 eV [1-4]. A wide band gap means ZnO has high optical transparency and luminescence in the visible and near-ultraviolet range of the spectrum. Therefore, it is usually used in optoelectronic devices including light-emitting diodes, photodetectors, solar cells, and p-n homojunctions [5-8]. A large exciton binding energy means the excitonic transition in case of ZnO nanoparticles is possible at room temperature [9-11].

ZnO nanoparticles are useful as antibacterial and antifungal when added into materials, including textiles, paints, and plastics [12 ,13]. Due to its bacteriostatic and fungistatic behavior, ZnO has been utilized in personal-care products and cosmetics [14, 15]. Because of its non-toxicity and suitability with skin, it is a convenient additive for textiles and other surfaces that meet the human body [16]. Other application areas of ZnO are gas sensors [17], chemical sensors [18-19], biosensors [20-21], superconductors [22] and, photocatalyst [23].

ZnO is one of the first semiconductors to prepare in pure form after Si and Ge and has the high heat capacity and heat conductivity, low thermal expansion and high melting temperature [24]. Many techniques have been used to produce ZnO nanoparticles for various applications such as chemical vapor deposition [25], pulsed laser deposition [26], molecular beam epitaxy [27], sputtering [28], hydrothermal synthesis [29], and oxidation of metallic zinc powder [30, 31], precipitation [32], sol-gel [33] and wet chemical synthesis [34]. Moreover, ZnO is environmentally friendly and easy to synthesize [35].

ZnO, as well as being produced without additives, has been prepared by many researchers by adding various elements such as Ru, Eu, Ce, Mg, Al, Ni, Sb and Mn [36-42]. Yttrium (Y) is another dopant for ZnO and some of the studies on Y-doped ZnO samples are given as follows. Kaya *et al.* [43] studied the mechanical properties of Y-doped ZnO samples prepared by a sol-gel method and they reported that Y-content increases the fracture toughness of ZnO. It was reported that the addition of Y into ZnO affects its optical properties, especially the optical band gap [44]. The photocatalytic activity in methylene blue degradation of Y-doped ZnO by microwave irradiation was investigated by Sanoop et al. [45]. Li et al. [46] reported that Y-doping into ZnO improves its gas sensing property. The gigantic piezoelectric response of Y-doped ZnO nanosheets prepared by wet chemical co-precipitation method was reported by Sinha et al. [47].

To the best of our knowledge, an available study related to the more detailed XRPD analysis on Y-containing ZnO samples synthesized via the combustion method has not been reported in the literature. For this reason, as well as their structural and thermal properties, we focused to determine the effects of Y-content on the crystal structure-related parameters of ZnO samples.

II. MATERIALS AND METHOD

All chemicals used in the combustion reaction of ZnO samples doped with Y at various amounts (*e.g.*, 0, 1, 3 and 5 at. %) were purchased from Sigma-Aldrich. Urea and distilled water were used as a fuel source and solvent, respectively. 100 mL solution of (40-*x*) mmol of zinc nitrate hexahydrate and *x* mmol of yttrium (III) nitrate hexahydrate was prepared in a beaker, where *x* is 0, 0.4, 1.2 and 2.0. According to the Y content, these samples were labelled as ZnO, 1YZnO, 3YZnO and 5YZnO, respectively. 10 mL of 0.2 M of urea was poured into each sample and these solutions were continuously stirred in a magnetic stirrer at room temperature. This was then followed by heating in a muffle furnace

at 500 °C for 30 mins to dry the solutions in the beakers. An ignition and dense smoke were observed after the boiling of each solution during this time. Dried powders were calcined in an electric furnace at 975 °C for 2 h, and the un-doped and Y-doped ZnO powders were obtained.

X-ray powder diffraction (XRPD) data at ambient temperature were collected by a Rigaku RadB-DMAX II model diffractometer. Fourier transform infrared (FTIR) spectra were recorded by a Perkin Elmer Spectrum One spectrophotometer in order to determine the functional groups in the samples using the KBr pellet method. The differential thermal analysis (Shimadzu DTA 50) and thermogravimetric analysis (Shimadzu TGA 50) were used to investigate the thermal behaviors of the as-synthesized ZnO samples under nitrogen atmosphere in the temperature range of 25-950 °C. The morphological investigations and elemental analyses of samples were carried out by using a LEO EVO 40xVP model scanning electron microscope (SEM) equipped with an energy dispersive X–ray (EDX, Röntech xflash) detector.

III. RESULTS AND DISCUSSION

A. XRPD ANALYSIS

XRPD profiles of pure and Y-containing ZnO samples in the 2θ range of 20 - 80° are shown in Fig.1. ZnO is known to adopt a wurtzite hexagonal crystal structure with a space group of $P6_3mc$ (JCPDS PDF No: 36-1451). Our XRPD data confirms that the synthetic method we employed leads to the formation of polycrystalline single-phase ZnO powder with wurtzite hexagonal structure symbolized with the ⅄ on the XRD patterns as reported in the literature. However, Y-containing ZnO samples were found to contain a small fraction of cubic yttrium oxide (Y_2O_3, JCPDS PDF No: 79-1716) shown with the ● symbol, impurity phase, clearly evident in the diffraction profiles shown in Fig. 1. Qualitative inspection of the XRPD profiles confirms that there is an increase in the impurity phase with increasing Y-content. This trend was previously reported by Ivanova *et al*. [48].

The sets of the Miller indices (*hkl*) belonging to (100), (002), (101), (102), (110), (103), (200), (112), (201), (004) and (202) planes were observed for each sample. The observed and calculated values of the distance for two adjacent plane (*d*) and 2θ angles are tabulated in Table 1. The calculated and observed *d* and 2θ values were found to be close to each other. This confirms the successful formation of polycrystalline hexagonal structure with a space group of $P6_3mc$.

We have calculated the crystallinity percent (X_C %) to quantitatively compare the effect of Y-content on crystallinity using the following equation [49]

$$X_C\% = \frac{\sum A_C}{\sum A_C + \sum A_A} \times 100 \quad (1)$$

here ΣA_C and ΣA_A are the total areas under crystal peaks and amorphous peaks, respectively. The crystallinity percent values of Y-doped ZnO samples are higher than that of pure ZnO (Table 2). Y-doping into ZnO improves its crystallinity and this result is in very good harmony with the reported one by Kumar et al. [50].
Using the Miller indices (*hkl*) and *d* values, the lattice parameters (*a* and *c*) and unit cell volume (*V*) were estimated using the following relations, respectively [51]:

$$\frac{1}{d^2} = \frac{4}{3}\left(\frac{h^2+hk+k^2}{a^2}\right) + \frac{l^2}{c^2} \quad (2)$$

$$V = 0.866a^2c \quad (3)$$

A gradual increase in both lattice parameters is observed with increasing Y-content. This is due to the difference between ionic radii of Zn^{2+} (0.074 nm) and Y^{3+} (0.092 nm) resulting in an increase in the lattice parameter(s), as well as the ionic imbalance, and is in good agreement with the literature [52-55].

To calculate the crystallite size for each ZnO sample, the following Scherrer (D_S) and Williamson-Hall (D_{WH}) equations were used, respectively [51, 56]

$$D_S = \frac{0.9\lambda}{\beta \cos\theta} \tag{4}$$

$$\beta \cos\theta = \frac{0.9\lambda}{D_{WH}} + 4\varepsilon \sin\theta \tag{5}$$

where β is the full width at half maximum, θ is the Bragg angle, λ is the X-ray wavelength and ε is the lattice strain. The D_{WH} and ε values were computed from the βcosθ vs. 4sinθ plots for each sample (Fig. 2). For the purpose of estimating the stress (σ) in the surface, the relation of the σ/Y was written in Eq. (5) instead of ε [56].

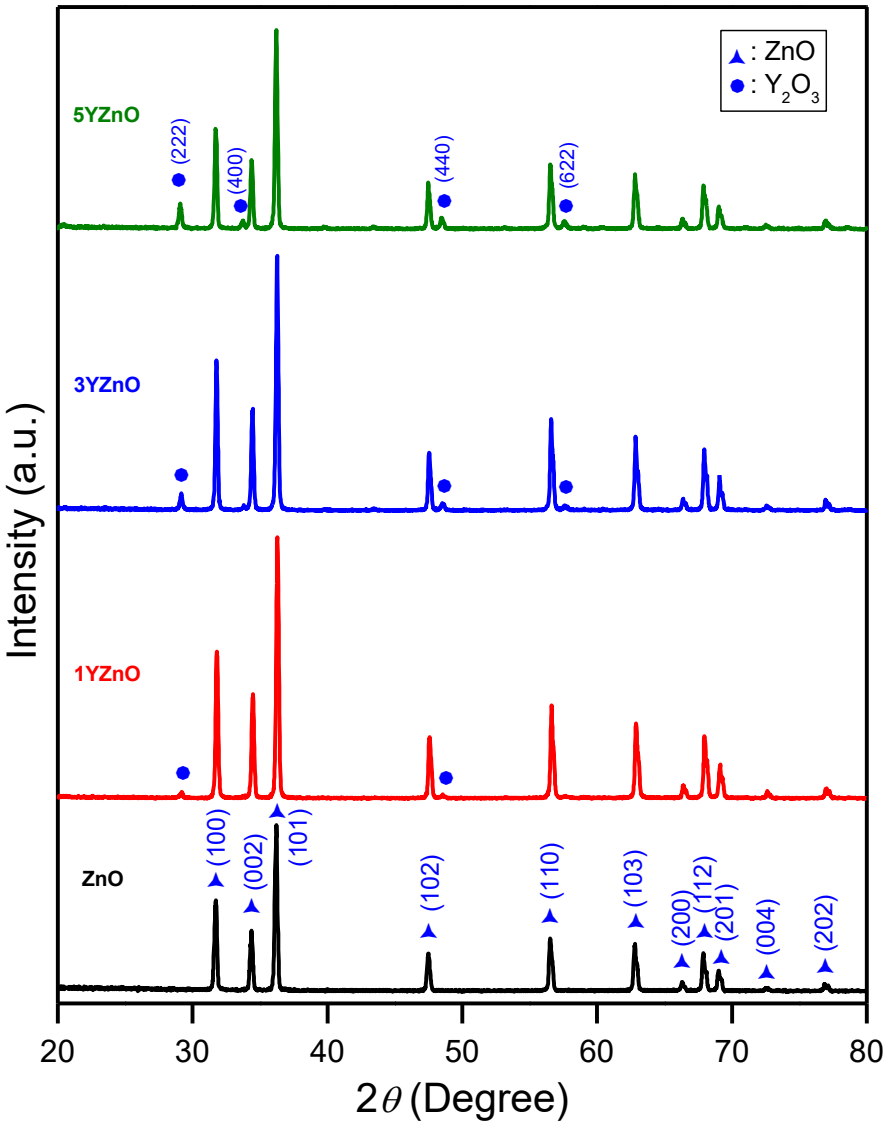

Figure 1. *XRPD patterns of the un-doped and Y-doped ZnO samples*

Table 1. *The observed and calculated values of the d and 2θ values for each sample*

Sample	*h*	*k*	*l*	d_{obs} (nm)	d_{cal} (nm)	Δd (nm)	$2\theta_{obs}$ (°)	$2\theta_{cal}$ (°)	$\Delta\theta$ (°)
ZnO	1	0	0	0.281863	0.281730	0.000133	31.720	31.735	-0.015
	0	0	2	0.260786	0.260527	0.000259	34.360	34.395	-0.035
	1	0	1	0.247809	0.247824	-0.000015	36.220	36.218	0.002
	1	0	2	0.191337	0.191278	0.000059	47.480	47.496	-0.016
	1	1	0	0.162691	0.162657	0.000034	56.520	56.533	-0.013
	1	0	3	0.147847	0.147847	0.000000	62.800	62.800	-0.000
	2	0	0	0.140865	0.140865	0.000000	66.300	66.300	-0.000
	1	1	2	0.137966	0.137974	-0.000008	67.880	67.876	0.004
	2	0	1	0.135963	0.135983	-0.000020	69.020	69.008	0.012
	0	0	4	0.130239	0.130264	-0.000025	72.520	72.504	0.016
	2	0	2	0.123903	0.123912	-0.000009	76.880	76.873	0.007
1YZnO	1	0	0	0.281172	0.281320	-0.000148	31.800	31.783	0.017
	0	0	2	0.259906	0.260134	-0.000228	34.480	34.449	0.031
	1	0	1	0.247413	0.247460	-0.000047	36.280	36.273	0.007
	1	0	2	0.190958	0.190993	-0.000035	47.580	47.571	0.009
	1	1	0	0.162374	0.162420	-0.000046	56.640	56.623	0.017
	1	0	3	0.147636	0.147626	0.000010	62.900	62.905	-0.005
	2	0	0	0.140715	0.140660	0.000055	66.380	66.409	-0.029
	1	1	2	0.137787	0.137771	0.000016	67.980	67.989	-0.009
	2	0	1	0.135756	0.135785	-0.000029	69.140	69.123	0.017
	0	0	4	0.130084	0.130067	0.000017	72.620	72.631	-0.011
	2	0	2	0.123739	0.123730	0.000009	77.000	77.007	-0.007
3YZnO	1	0	0	0.281517	0.281470	0.000047	31.760	31.765	-0.005
	0	0	2	0.260199	0.260321	-0.000122	34.440	34.423	0.017
	1	0	1	0.247545	0.247603	-0.000058	36.260	36.251	0.009
	1	0	2	0.191109	0.191115	-0.000006	47.540	47.539	0.001
	1	1	0	0.162480	0.162507	-0.000027	56.600	56.590	0.010
	1	0	3	0.147720	0.147725	-0.000005	62.860	62.858	0.002
	2	0	0	0.140752	0.140735	0.000017	66.360	66.369	-0.009
	1	1	2	0.137823	0.137852	-0.000029	67.960	67.944	0.016
	2	0	1	0.135859	0.135859	0.000000	69.080	69.080	-0.000
	0	0	4	0.130177	0.130161	0.000016	72.560	72.570	-0.010
	2	0	2	0.123821	0.123801	0.000020	76.940	76.954	-0.014
5YZnO	1	0	0	0.282036	0.281656	0.000380	31.700	31.744	-0.044
	0	0	2	0.260639	0.260496	0.000143	34.380	34.400	-0.020
	1	0	1	0.247942	0.247767	0.000175	36.200	36.226	-0.026
	1	0	2	0.191337	0.191242	0.000095	47.480	47.505	-0.025
	1	1	0	0.162638	0.162614	0.000024	56.540	56.549	-0.009
	1	0	3	0.147805	0.147823	-0.000018	62.820	62.811	0.009
	2	0	0	0.140790	0.140828	-0.000038	66.340	66.320	0.020
	1	1	2	0.137930	0.137943	-0.000013	67.900	67.893	0.007
	2	0	1	0.135963	0.135949	0.000014	69.020	69.028	-0.008
	0	0	4	0.130239	0.130248	-0.000009	72.520	72.514	0.006
	2	0	2	0.123848	0.123883	-0.000035	76.920	76.894	0.026

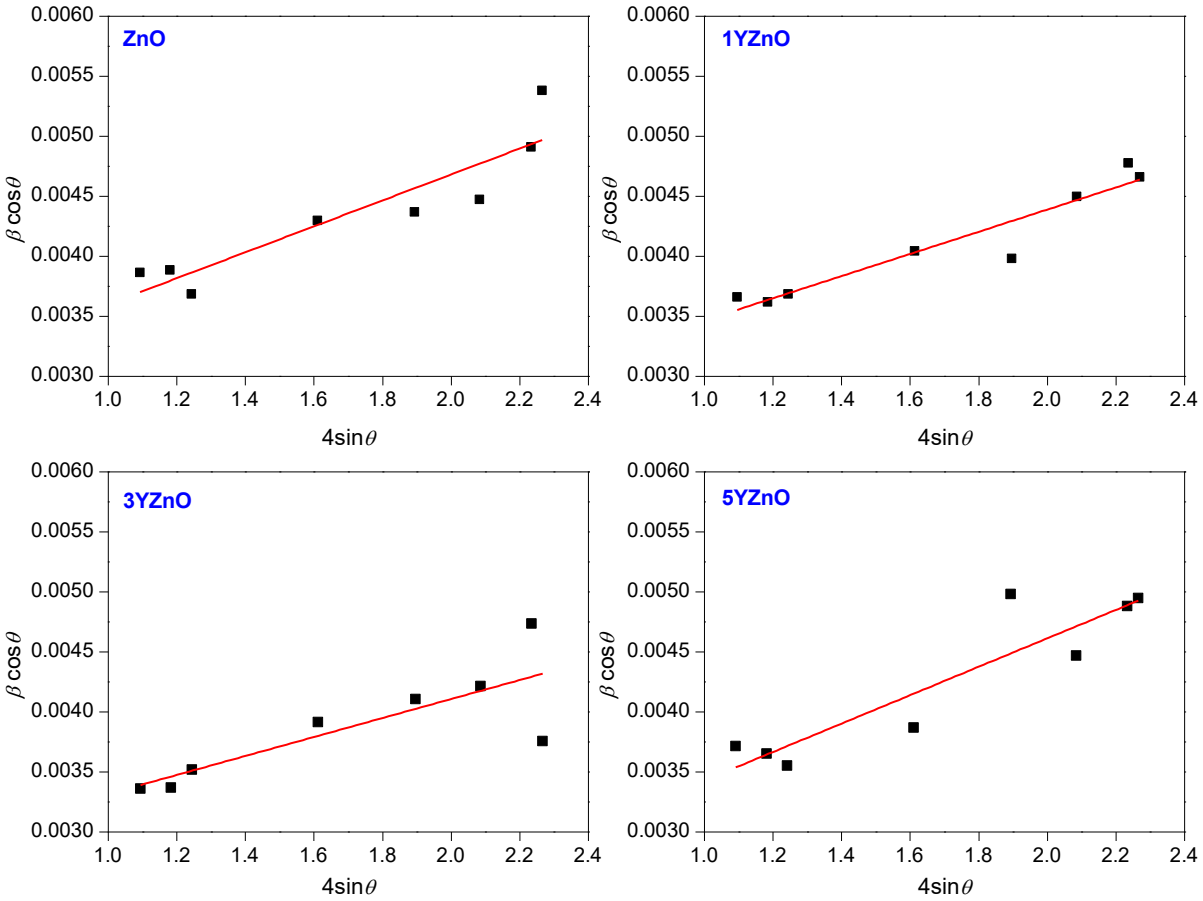

Figure 2. *The βcosθ vs. 4sinθ plots for each sample.*

$$\beta \cos\theta = \frac{0.9\lambda}{D_{WH}} + \frac{4\sigma \sin\theta}{Y} \tag{6}$$

where Y is Young's modulus and calculated using the following relation.

$$Y = \frac{\left[h^2+\frac{(h+2k)^2}{3}+\left(\frac{al}{c}\right)^2\right]^2}{s_{11}\left(h^2+\frac{(h+2k)^2}{3}\right)^2+s_{33}\left(\frac{al}{c}\right)^4+(2s_{13}+s_{44})\left(h^2+\frac{(h+2k)^2}{3}\right)\left(\frac{al}{c}\right)^2} \tag{7}$$

here the values of s_{11}=7.858×10^{-12} m^{2}N^{-1}, s_{13}=−2.206×10^{-12} m^{2}N^{-1}, s_{33}=6.940×10^{-12} m^{2}N^{-1} and s_{44}=23.57×10^{-12} m^{2}N^{-1} are known as the elastic compliances [56]. The slope of the $\beta cos\theta$ vs. $4sin\theta/Y$ graphs plotted in Fig. 3 corresponds to the σ value.

Eq. (5) can be modified by using the relation of $\varepsilon = (2u/Y)^{1/2}$ to calculate the energy density (u) values for all the samples.

$$\beta \cos\theta = \frac{0.9\lambda}{D_{WH}} + 4 \sin\theta \left(\frac{2u}{Y}\right)^{1/2} \tag{8}$$

With the aid of the $\beta cos\theta$ vs. $2^{5/2} sin\theta\ Y^{-1/2}$ plot shown in Fig. 4, the u values for each sample were calculated.

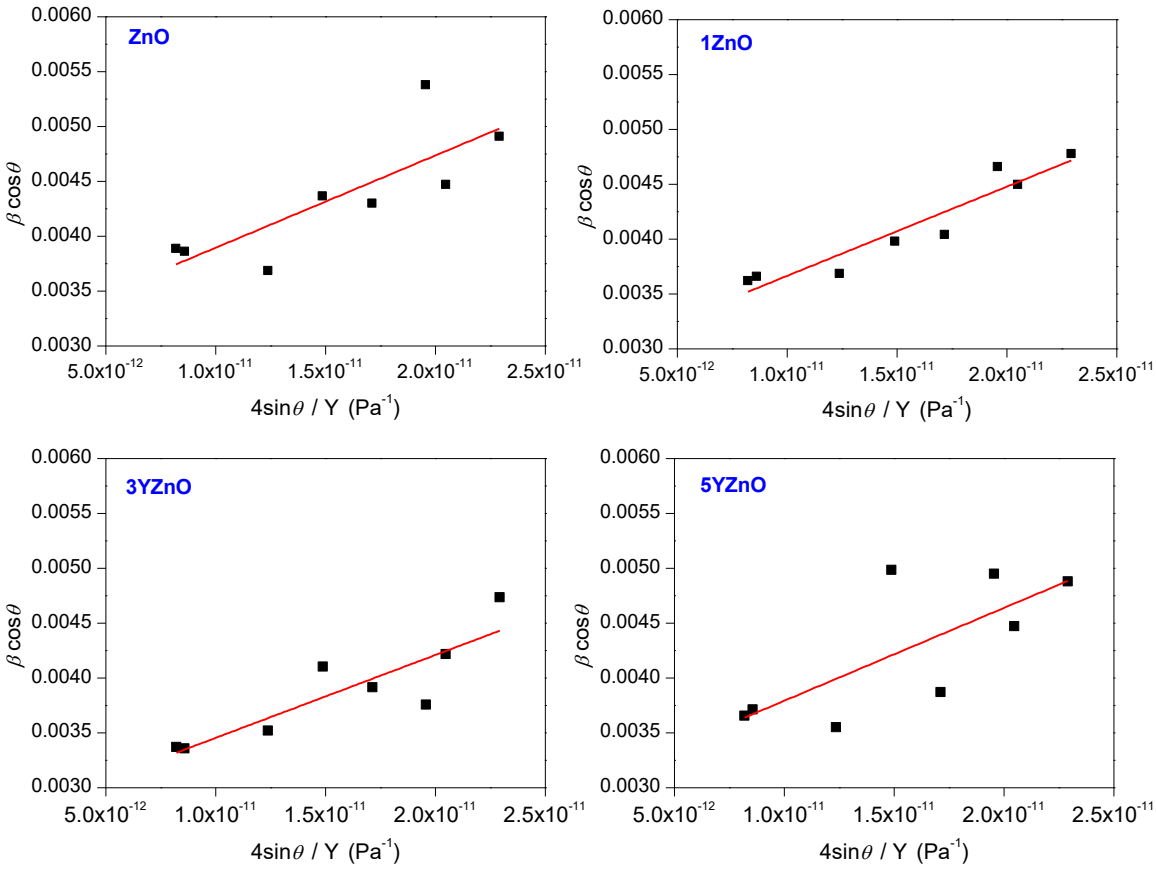

Figure 3. *The βcosθ vs. 4sinθ/Y graphs of the as-synthesized ZnO samples*

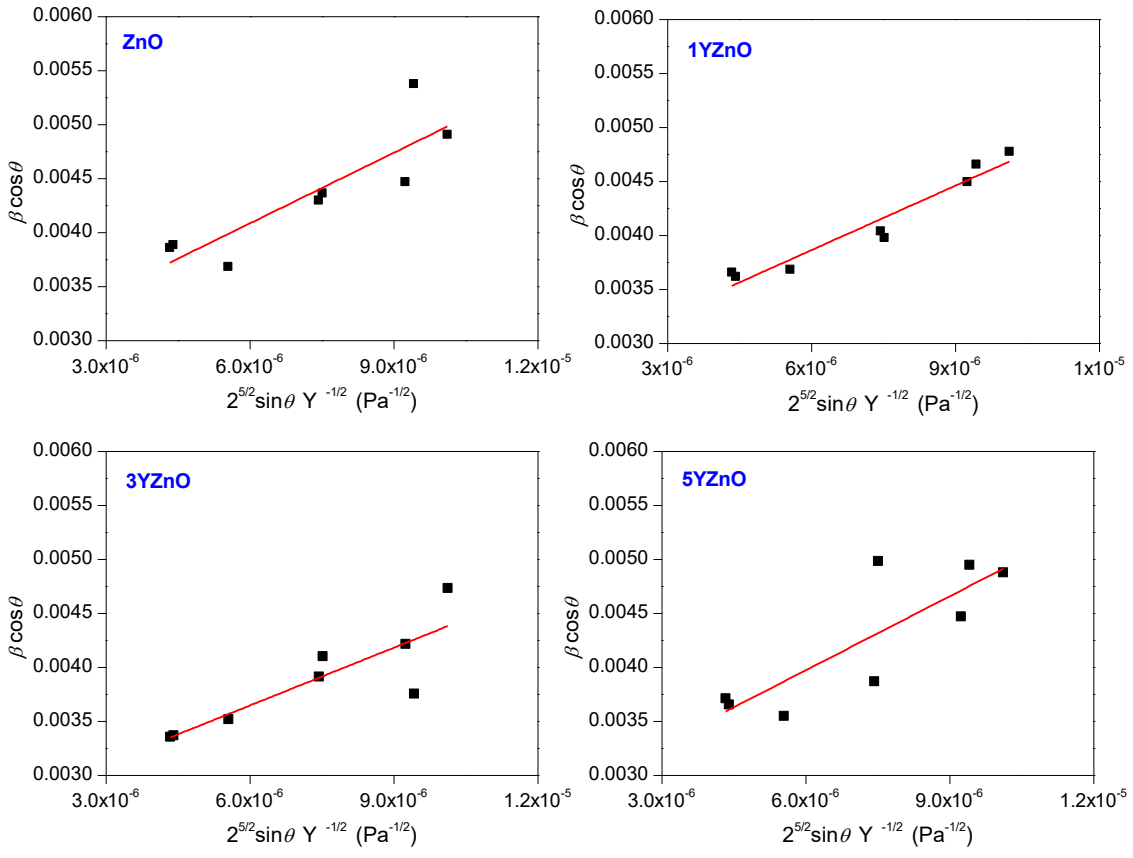

Figure 4. *The βcosθ vs. $2^{5/2}$sinθ $Y^{-1/2}$ plots for the un-doped and Y-doped ZnO samples*

The bond length (L) between Zn and O was estimated from the following relation [57]

$$L = \sqrt{\frac{a^2}{3} + c^2\left(0.25 - \frac{a^2}{3c^2}\right)^2} \quad (9)$$

The L value gradually increases with increasing Y content as can be seen from Table 2. The trend of the increase in the L value with the increasing amount of Y is a very good agreement with Anandan and Muthukumaran [58].

Atomic packing factor (*APF*) was estimated by using the following relation [59]

$$APF\% = \frac{2\pi a}{3\sqrt{3}c} \times 100 \quad (10)$$

All the *APF* % values tabulated in Table 2 are higher than that of the standard one belonging to the hexagonal structure (74%). Additionally, the doping of Y causes very small decreases, which can be neglected, in the *APF* % in comparison to the un-doped ZnO.

Table 2. *The detailed XRPD analysis report of the un-doped and Y-doped ZnO samples.*

	ZnO	**1YZnO**	**3YZnO**	**5YZnO**
ZnO phase (%)	100	99.1	96.2	93.3
Y_2O_3 phase (%)	-	0.9	3.8	6.7
X_C%	93.9	95.8	95.7	94.9
D_S (nm)	36.41	37.96	40.63	38.13
D_{WH} (nm)	46.81	46.90	49.08	48.53
***a* (nm)**	0.32477	0.32484	0.32501	0.32523
***c* (nm)**	0.52010	0.52027	0.52064	0.52099
c* / *a	1.60144	1.60162	1.60192	1.60191
***V* (nm^3)**	0.04751	0.04754	0.04763	0.04772
***L* (nm)**	0.19762	0.19767	0.19779	0.19792
$\varepsilon \times 10^{-3}$	1.08	0.92	0.79	1.18
σ (MPa)	84.12	81.33	75.56	84.66
***u* (kJ m^{-3})**	47.46	35.60	31.74	52.22
***APF*%**	75.47	75.46	75.45	75.45

B. FTIR RESULTS

FTIR spectra of samples are shown in Fig. 5. The observed bands and their assignments are as follows: the bands detected at 421 and 1055 cm^{-1} are associated with Zn-O bonds belonging to the ZnO structure [60, 61]. The weak bands for each sample detected at about 2000-2400 cm^{-1} are related to the stretching mode of C-O bond of CO_2 group, and another one observed at 2921 cm^{-1} is attributed to the stretching vibration modes of C-H bond, most probably arising from trace content of urea which was used a fuel for the combustion reaction [62, 63].

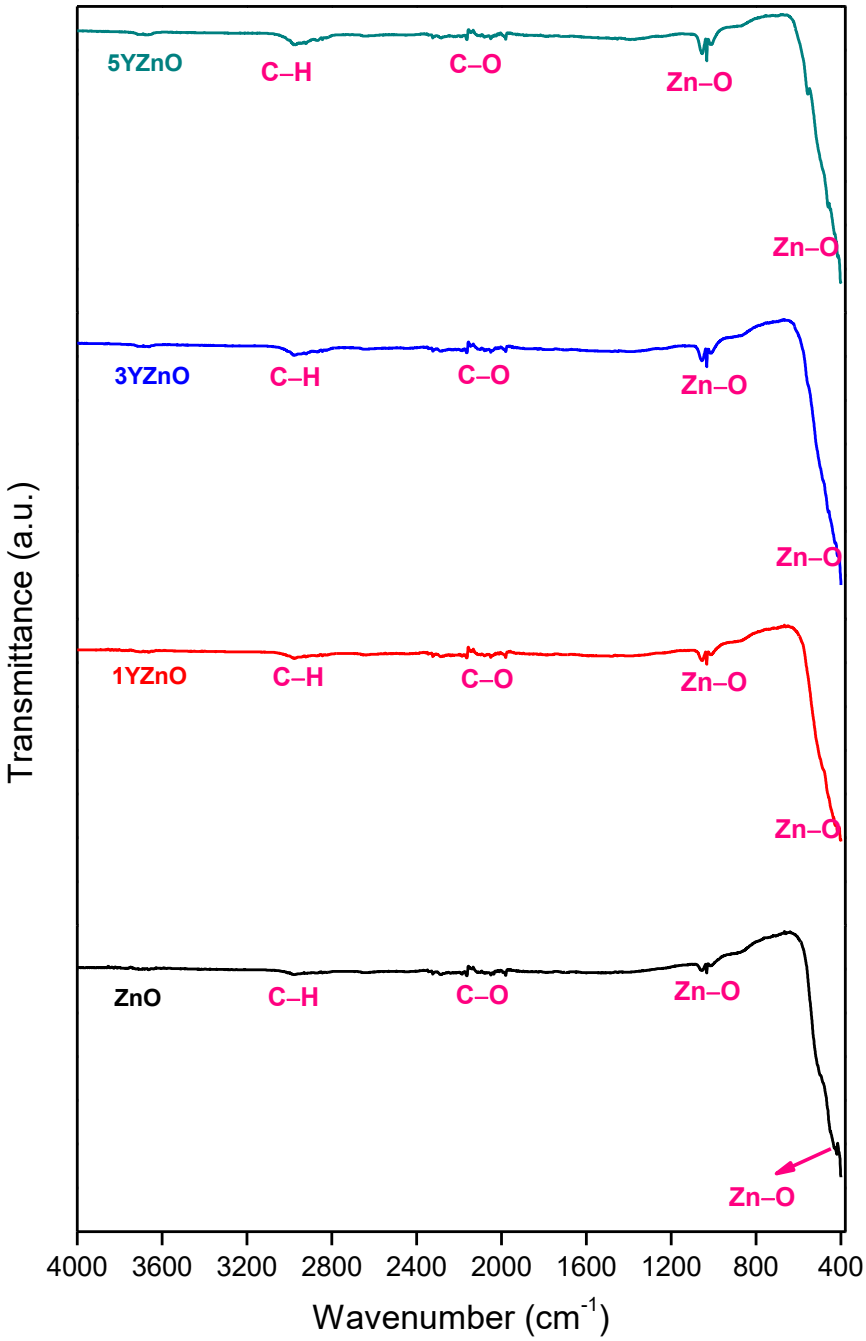

Figure 5. *FTIR spectra of the as-prepared ZnO samples*

C. THERMAL CHARACTERIZATION

DTA and TGA results are plotted in Fig. 6 and Fig. 7, respectively. As can be seen from the DTA thermograms in Fig. 6, each sample is thermally stable in the temperature range of 25 - 950 °C. The TGA results shown in Fig. 7 present the mass change with increasing temperature for each sample. For the un-doped ZnO, the mass loss starts at a temperature of 418 °C and reaches the maximum value of 1.48% at 577 °C. The mass gain of 0.25% is observed from 577 to 950 °C. The total mass loss for the un-doped ZnO is 1.23% from room temperature to 950 °C. For the 1YZnO sample, the mass loss starts at 538 °C and its maximum value (1.12%) is detected at 693 °C. Like the un-doped ZnO, the mass gain begins and continues after this temperature. Compared to the starting mass, the value of 0.18% mass gain is observed. For the ZnO and 1YZnO samples, the as-observed mass losses are associated with the

elimination of the adsorbed substances on the oxide surface [64]. For both 3YZnO and 5YZnO samples, no mass loss is observed. A continued mass gain is detected until 950 °C for both samples. The total mass gain is found to be 1.77% and 2.24% for 3YZnO and 5YZnO, respectively. The increase in the mass can be related to the introduction of oxygen from the atmosphere into the samples [65].

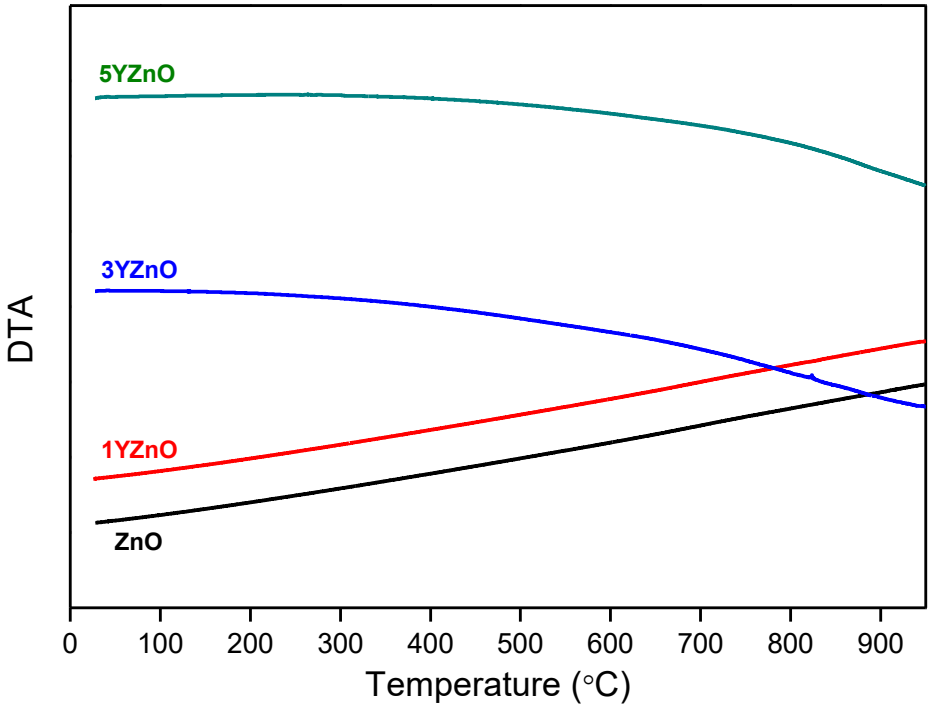

Figure 6. *DTA thermograms of the un-doped and Y-doped ZnO samples*

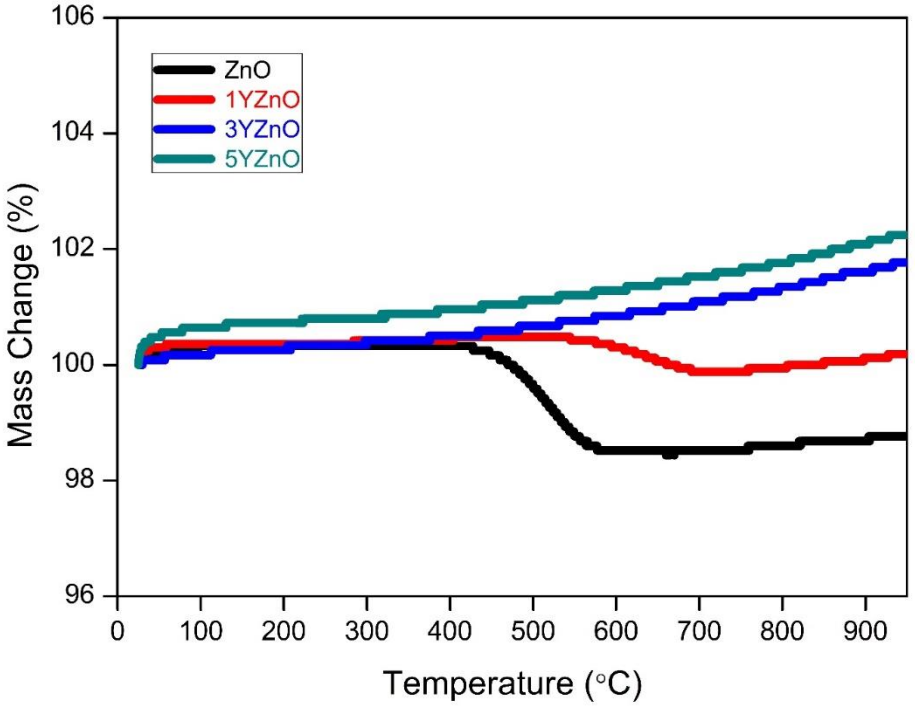

Figure 7. *TGA graphs of the samples*

D. MORPHOLOGICAL AND ELEMENTAL ANALYSIS

The morphologies of the samples are shown in Fig. 8. A randomly-oriented pyramidal crystal growth is observed from the SEM images. The formation of ZnO pyramids is associated with the anisotropic growth of various crystal facets belonging to ZnO [66]. Remarkable effects of the influence of Y can be seen from the SEM observations. The dimensions of the pyramidal grains of the rest samples are smaller than that of the un-doped ZnO, and the as-observed decrease in the grain size of ZnO is in a very good agreement with Kaya et al. [43]. EDX results confirm the introduction of Y without any impurity in the samples.

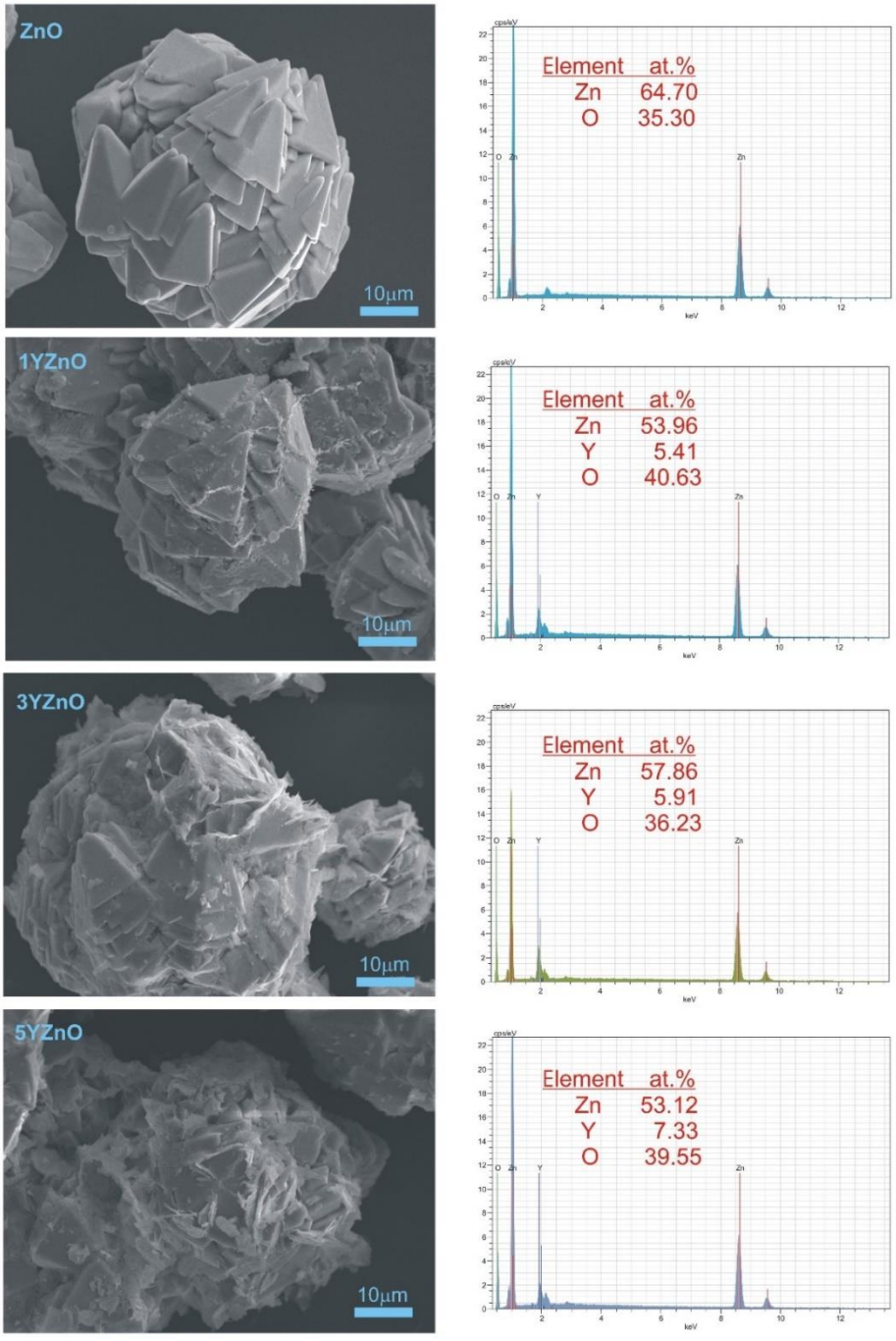

Figure 8. *SEM images and EDX reports for each sample*

IV. CONCLUSIONS

The un-doped and Y-doped ZnO samples, having a low production cost, were easily and successfully prepared using the combustion synthesis. The formation of the Y_2O_3 phase by adding Y into the ZnO structure was observed. The percent of the secondary phase of Y_2O_3 increases gradually with the increasing amount of Y. The amount of Y affects significantly the crystal structure related parameters. As well as the bond length and unit cell volume of Zn-O, a gradual increase in both lattice parameters is observed with increasing Y-content. The crystallinity values of the Y-doped ZnO samples are higher than that of the un-doped ZnO. The atomic packing factor is affected by the adding of Y. All samples are found to be thermally stable in the temperature range interval of 25-950 °C. The mass change mechanism of ZnO can be controlled by Y-content because an increasing amount of Y causes a gradual increase in the mass gain percent. The synthetic technique we employed for this study leads to the emergence of randomly-oriented pyramidal morphology in ZnO/Y-doped ZnO powders. No other impurities were detected besides the secondary impurity phase of Y_2O_3.

V. REFERENCES

[1] C.M. Lieber, "One-dimensional nanostructures," *Chemistry, Physics & Applications. Solid State Commun*., vol. 107, pp. 607-616, 1998.

[2] Ö.A. Yıldırım, H.E. Unalan, C. Durucan, "Highly efficient room temperature synthesis of silver-doped zinc oxide (ZnO:Ag) nanoparticles: Structural, optical, and photocatalytic properties," *J. Am. Ceram. Soc*, vol. 96, pp.766-773, 2013.

[3] X.B. Wang, C. Song, K.W. Geng, F. Zeng, F. Pan, "Luminescence and Raman scattering properties of Ag-doped ZnO films," *J. Phys. D: Appl. Phys*, vol. 39, pp. 4992, 2006.

[4] E. Mosquera, J. Bernal, R.A. Zarate, F. Mendoza, R.S. Katiyar, G. Morell, "Growth and electron field-emission of single-crystalline ZnO nanowires," *Mater. Lett*, vol. 93, pp. 326-329, 2013.

[5] L. Zhao, P.F. Lu, Z.Y. Yu, X.T. Guo, Y. Shen, H. Ye, G.F. Yuan, L. Zhang, "The electronic and magnetic properties of (Mn,N)-codoped ZnO from first principles," *J. Appl. Phys*, vol. 108 pp. 113924, 2010.

[6] S. Shao, K. Zheng, K. Zidek, P. Chabera, T. Pullerits, F. Zhang, "Optimizing ZnO nanoparticle surface for bulk heterojunction hybrid solar cells," *Sol. Energy Mater. Sol. Cells*, vol. 118, pp. 43-47, 2013.

[7] S. Venkataprasad Bhat, A. Govindaraj, C.N.R. Rao, "Hybrid solar cell based on P3HT–ZnO nanoparticle blend in the inverted device configuration," *Sol. Energy Mater. Sol. Cells*, vol. 95, pp. 2318-2321, 2011.

[8] J. Luo, Y. Wang, Q. Zhang, "Progress in perovskite solar cells based on ZnO nanostructures," *Sol. Energy*, vol. 163, pp. 289-306, 2018.

[9] H. Yıldırım, "Exciton binding and excitonic transition energies in wurtzite $Zn_{1-x}Cd_xO$/ZnO quantum wells" *Superlattices and Microstruct*, vol. 120, pp. 344-352, 2018.

[10] W.Q. Peng, S.C. Qu, G.W. Cong, Z.G. Wang, "Structure and visible luminescence of ZnO nanoparticles," *Mater. Sci. Semic. Proc*, vol. 9, pp. 156, 2006.

[11] Q. Yu, W. Fu, C. Yu, H. Yang, R. Wei, Y. Sui, Y. Lui, Z. Lui, M. Li, G. Wang, C. Shao, Y. Lui, G.Zou, "Structural, electrical and optical properties of yttrium-doped ZnO thin films prepared by sol–gel method," *J. Phys. D: Appl. Phy.*, vol. 40, pp. 5592, 2007.

[12] Y. Xie, Y. He, P.L. Irwin, T. Jin, X. Shi, "Antibacterial activity and mechanism of action of zinc oxide nanoparticles against Campylobacter jejuni," *Appl. Environ. Microbiol*, vol. 77, pp. 2325-2331, 2011.

[13] L. He, Y. Liu, A. Mustapha, M. Lin, "Antifungal activity of zinc oxide nanoparticles against Botrytis cinerea and Penicillium expansum," *Microbiol. Res*, vol. 166, pp. 207-215, 2011.

[14] V.B. Patravale, S.D. Mandawgade, "Novel cosmetic delivery systems: an application update," *Int. J. Cosmet. Sci*, vol. 30, pp. 19-33, 2008.

[15] Y.K. Mishra, R. Adelung, "ZnO tetrapod materials for functional applications," *Materials Today*, vol. 21, pp. 631-651, 2018.

[16] N. Vigneshwaran, S. Kumar, A. Kathe, P. Varadarajan, V. Prasad, "Functional finishing of cotton fabrics using zinc oxide–soluble starch nanocomposites," *Nanotechnology*, vol. 17, pp. 5087-5095, 2006.

[17] S.K. Gupta, A. Joshi, M. Kaur, "Development of gas sensors using ZnO nanostructures". *J. Chem. Sci.*, vol. 122, pp. 57-62, 2010.

[18] K. Diao, J. Xiao, Z. Zheng, X. Cui, "Enhanced sensing performance and mechanism of CuO nanoparticle-loaded ZnO nanowires: Comparison with ZnO-CuO core-shell nanowires," *Appl. Surf. Sci*, vol. 459, pp. 630-638, 2018.

[19] Z. Fan, J.G. Lu, "Chemical Sensing with ZnO Nanowire Field-Effect Transistor" *IEEE Trans. Nanotechnol*, vol. 5, pp. 393-396, 2006.

[20] Z. Zhao, W. Lei, X. Zhang, B. Wang, H. Jian, "ZnO-based amperometric enzyme biosensors," *Sensors*, vol. 10, pp. 1216-1231, 2010.

[21] C.X. Xu, C. Yang, B.X. Gu, S.J. Fang, "Nanostructured ZnO for biosensing applications," *Chin Sci. Bull*, vol. 58, pp. 2563-2566, 2013.

[22] P. Sharma, A. Gupta, K.V. Rao, F.J. Owens, R. Sharma, R. Ahuja, J.M. Osorio Guillen, B. Johansson, G.A. Gehring, "Ferromagnetism above room temperature in bulk and transparent thin films of Mn-doped ZnO," *Nature Mater*, vol. 2, pp. 673-637, 2003.

[23] A. Bagabas, A. Alshammari, M.F.A. Aboud, H. Kosslick, "Room-temperature synthesis of zinc oxide nanoparticles in different media and their application in cyanide photodegradation," *Nanoscale Res. Lett*, vol. 8, pp. 516, 2013.

[24] F. Porter, "Zinc Handbook: Properties, Processing, and Use in Design, Marcel Dekker," New York, 1991.

[25] M.M.C. Chou, D.R. Hang, C. Chen, S.C. Wang, C.Y. Lee, "Nonpolar a-plane ZnO growth and nucleation mechanism on (100) (La, Sr) (Al, Ta)O3 substrate". *Mater. Chem. Phys*, vol. 12, pp. 791–795, 2011.

[26] B.L. Zhu, X.Z. Zhao, F.H. Suc, G.H. Li, X.G. Wu, J. Wu, R. Wu, "Low temperature annealing effects on the structure and optical properties of ZnO films grown by pulsed laser deposition," *Vacuum*, vol. 84, pp. 1280–1286, 2010.

[27] Z. Yang, J.H. Lim, S. Chu, Z. Zuo, J.L. Liu, "Study of the effect of plasma power on ZnO thin films growth using electron cyclotron resonance plasma assisted molecular-beam epitaxy," *Appl. Surf. Sci.*, vol. 255, pp. 3375–3380, 2008.

[28] S. Sohal, Y. Alivov, Z. Fan, M. Holtz, "Role of phonons in the optical properties of magnetron sputtered ZnO studied by resonance Raman and photoluminescence," *J. Appl. Phys*., vol. 108, pp. 053507–053511, 2010.

[29] C. Wu, L. Shen, Q. Huang, Y.C. Zhang, "Synthesis of Na-doped ZnO nanowires and their antibacterial properties," *Powder Technol.*, vol. 205, pp. 137–142, 2011.

[30] S.S. Chang, C.H. Park, S.W. Park, "Improved photoluminescence properties of oxidized anodically etched porous Zn," *Mater. Chem. Phys.*, vol. 79, pp. 9-14, 2003.

[31] Z. Xiao, M. Okada, G. Han, M. Ichimiya, K. Michibayashi, T. Itoh, Y. Neo, T. Aoki, H. Mimura, "Undoped ZnO phosphor with high luminescence efficiency grown by thermal oxidation," *J. Appl. Phys.*, vol. 104, pp. 073512-073514, 2008.

[32] S. Chen, V. Rangari, A. Gedanken, A. Zaban, "Sonochemical synthesis of crystalline nanoporous zinc oxide spheres and their application in dye sensitized solar cells," *Isr. J. Chem.*, vol. 41, pp. 51-54, 2001.

[33] N. Singh, D. Dhruvashi Kaur, R.M. Mehra, A. Kapoor, "Effect of ageing in structural properties of ZnO nanoparticles with pH variation for application in solar cells," *The Open Renewable Energy Journal*, vol. 5, pp. 15-18, 2012.

[34] J. Zhu, D. Deng, "Ammonia-assisted wet-chemical synthesis of ZnO microrod arrays on substrates for microdroplet transfer," *Langmuir*, vol. 33, pp. 6143-6150 2017.

[35] Y.L. Wu, A.I.Y. Tok, F.Y.C. Boey, X.T. Zeng, X. H. Zhang, "Surface modification of ZnO nanocrystals," *Appl. Surf. Sci.*, vol. 253, pp. 5473-5479, 2007.

[36] I. Iwantono, R. Yuda, S.K. Md. Saad, M.Y. Abd. Rahman, A.A. Umar, "Structural and properties transformation in ZnO hexagonal nanorod by ruthenium doping and its effect on DSSCs power conversion efficiency," *Superlattices Microstruct*, vol. 123, pp. 119-128, 2018.

[37] P. Mohanty, B. Kim, J. Park, "Synthesis of single crystalline europium-doped ZnO nanowires," *Mater. Sci. Eng. B.*, vol. 138, pp. 224-227, 2007.

[38] D. Gao, J. Zhang, B. Lyu, L. Lyu, J. Ma, L. Yang, "Poly (quaternary ammonium salt-epoxy) grafted onto Ce doped ZnO composite: An enhanced and durable antibacterial agent," *Carbohydr. Polym.*, vol. 200, pp. 221-228, 2018.

[39] P. Giri, P. Chakrabarti, "Effect of Mg doping in ZnO buffer layer on ZnO thin film devices for electronic applications," *Superlattices Microstruct.*, vol. 93, pp. 248-260, 2016.

[40] H. Benzarouk, A. Drici, M. Mekhnache, A. Amara, M. Guerionune, J.C. Bernede, H. Bendjffal, "Effect of different dopant elements (Al, Mg and Ni) on microstructural, optical and electrochemical properties of ZnO thin films deposited by spray pyrolysis (SP)," *Superlattices Microstruct.*, vol. 52, pp. 594-604, 2012.

[41] S. Nasser, H. Elhouichet, "Production of acceptor complexes in sol-gel ZnO thin films by Sb doping," *J. Lumin.*, vol. 196, pp. 11-19, 2018.

[42] M.V. Gallegos, M.A. Peluso, H. Thomas, L.C. Damonte, J.E. Sambeth, "Structural and optical properties of ZnO and manganese-doped ZnO," *J. Alloys Compd.*, vol. 689, pp. 416-424, 2016.

[43] S. Kaya, D. Akcan, O. Ozturk, L. Arda, "Enhanced mechanical properties of yttrium doped ZnO nanoparticles as determined by instrumented indentation technique," *Ceram. Int.*, vol. 44, pp. 10306-10314, 2018.

[44] K. Siraj, J.Z. Hashmi, S. Naseem, M.S. Rafique, S. Shaukat, "Microstructure and optical properties of rare-earth doped ZnO thin films," *Mater. Today: Proc.*, vol. 2, pp. 5365-5372, 2015.

[45] P.K. Sanoop, S. Anas, S. Ananthakumar, V. Gunasekar, R. Saravanan, P. Ponnusami, "Synthesis of yttrium doped nanocrystalline ZnO and its photocatalytic activity in methylene blue degradation," *Arabian J. Chem.*, vol. 9, pp. S1618-S1626, 2016.

[46] X.B. Li, Q.Q. Zhang, S.Y. Ma, G.X. Wan, F.M. Li, X.L. Xu, "Microstructure optimization and gas sensing improvement of ZnO spherical structure through yttrium doping," *Sens. Actuators B.*, vol. 195, pp. 526-533, 2014.

[47] N. Sinha, S. Goel, A.J. Joseph, H. Yadav, K. Batra, M.K. Gupta, B. Kumar, "Y-doped ZnO nanosheets: Gigantic piezoelectric response for an ultra-sensitive flexible piezoelectric nanogenerator," *Ceram. Int.*, vol. 44, pp. 8582-8590, 2018.

[48] T. Ivanova, A. Harizanova, T. Koutzarova, B. Vertruyen, "Sol-gel derived ZnO:Y nanostructured films: Structural and optical study," *Colloids Surf. A.*, vol. 532, pp. 363-368, 2017.

[49] O. Kaygili, "Synthesis and characterization of Na2O–CaO–SiO2 glass–ceramic," *J. Therm. Anal. Calorim.*, vol. 117, pp. 223-227, 2014.

[50] M. Kumar, H. Jeong, A. Kumar, B.P. Singh, D. Lee, "Magnetron-sputtered high performance Y-doped ZnO thin film transistors fabricated at room temperature," *Mater. Sci. Semicond. Process.*, vol. 71, pp. 204-208, 2017.

[51] B.D. Cullity, "Elements of X–ray Diffraction. Addison–Wesley Publishing Company," Massachusetts. 1978.

[52] S. Heo, S.K. Sharma, S. Lee, Y. Lee, C. Kim, B. Lee, H. Lee, D.Y. Kim, "Effects of Y contents on surface, structural, optical, and electrical properties for Y-doped ZnO thin films," *Thin Solid Films.*, vol. 558, pp. 27-30, 2014.

[53] S.K. Sharma, D.Y. Kim, "Microstructure and optical properties of yttrium-doped zinc oxide (YZO) nanobolts synthesized by hydrothermal method," *J. Mater. Sci. Technol.*, vol. 32 pp. 12-16, 2016.

[54] J.Q. Wen, J.M. Zhang, Z.Q. Li, "Structural and electronic properties of Y doped ZnO with different Y concentration," *Optik*, vol. 156, pp. 297-302, 2018.

[55] M. Gao, J. Yang, L. Yang, Y. Zhang, J. Lang, H. Liu, H. Fan, Y. Sun, Z. Zhang, H. Song, "Enhancement of optical properties and donor-related emissions in Y-doped ZnO," *Superlattices Microstruct.*, vol. 52, pp. 84-91, 2012.

[56] O. Kaygili, I. Ercan, T. Ates, S. Keser, C. Orek, B. Gunduz, T. Seckin, N. Bulut, L. Banares, "An experimental and theoretical investigation of the structure of synthesized ZnO powder," *Chem. Phys.*, vol. 513, pp. 273-279, 2018.

[57] U. Seetawan, S. Jugsujinda, T. Seetawan, A. Ratchasin, C. Euvananont, C. Junin, C. Thanachayanont, P. Chainaronk, "Effect of calcinations temperature on crystallography and nanoparticles in ZnO disk," *Mater. Sci. Appl.*, vol. 2, pp. 1302-1306, 2011.

[58] S. Anandan, S. "Muthukumaran, Influence of yttrium on optical, structural and photoluminescence properties of ZnO nanopowders by sol–gel method," *Opt. Mater.*, vol. 35, pp. 2241-2249, 2013.

[59] P. Kumar, B.K. Singh, B.N. Pal, P.C. Pandey, "Correlation between structural, optical and magnetic properties of Mn-doped ZnO," *Appl. Phys. A.*, vol. 122, pp. 740, 2016.

[60] R. Joshi, "Facile photochemical synthesis of ZnO nanoparticles in aqueous solution without capping agents," *Materialia.*, vol. 2, pp. 104-110, 2018.

[61] S. Vijayakumar, B. Vaseeharan, "Antibiofilm, anti cancer and ecotoxicity properties of collagen based ZnO nanoparticles," *Adv. Powder Technol.*, vol. 29, pp. 2331-2345, 2018.

[62] M. Gharagozlou, S. Naghibi, "Sensitization of ZnO nanoparticles by metal–free phthalocyanine". *J. Lumin.*, vol. 196, pp. 64-68, 2018.

[63] A. Dhanalakshmi, A. Palanimurugan, B. Natarajan, "Efficacy of saccharides bio-template on structural, morphological, optical and antibacterial property of ZnO nanoparticles," *Mater. Sci. Eng. C.*, vol. 90, pp. 95-103, 2018.

[64] L.G. da Trindade, G.B. Minervino, A.B. Trench, M.H. Carvalho, M. Assis, M.S. Li, A.J.A. de Oliveira, E.C. Pereira, T.M. Mazzo, E. Longo, "Influence of ionic liquid on the photoelectrochemical properties of ZnO particles," Ceram. Int., vol. 44, pp. 10393-10401, 2018.

[65] G. Wu, Z. Jia, Y. Cheng, H. Zhang, X. Zhou, H. Wu, "Easy synthesis of multi-shelled ZnO hollow spheres and their conversion into hedgehog-like ZnO hollow spheres with superior rate performance for lithium ion batteries," *Appl. Surf. Sci.*, vol. 464, pp. 472-478, 2019.

[66] P.K. Samanta, S. Basak, "Electrochemical growth of hexagonal ZnO pyramids and their optical property," *Mater. Lett.*, vol. 83, pp. 97-99, 2012.